CrossMark

RESEARCH ARTICLE

Photocatalytic degradation of humic acids using substrate-supported Fe^{3+}-doped TiO_2 nanotubes under UV/O_3 for water purification

Rongfang Yuan[1] · Beihai Zhou[1] · Xuemin Zhang[1] · Huanhuan Guan[1]

Abstract In this paper, Fe^{3+}-doped TiO_2 nanotubes (Fe-TNTs) were successfully synthesized using hydrothermal method. Four different types of substrates, more specifically, ceramsite, zeolite, activated alumina, and activated carbon (AC), have been investigated in the study. The substrate-supported Fe-TNTs were used to effectively decompose humic acids (HAs) in water under O_3/UV conditions. The experiment results show that the highest photocatalytic activity was obtained in the presence of AC-supported 1.0 atomic percent (at.%) Fe-TNTs calcined at 500 °C, as HAs was removed by 97.4 %, with a pseudo-first-order rate constant of 0.126/min. The removal efficiencies of HAs reduced when the catalysts was repeatedly used, since the amount of adsorption sites of the supporting substrates decreased. However, even after the catalyst was repeatedly used for five times, the removal efficiency of HAs in the presence of AC-supported catalyst, which was 78.5 %, was still sufficient in water treatment. The enhanced photocatalytic activity of AC-supported Fe-TNTs was related to a synergistic effect of AC adsorption and Fe-TNT photocatalytic ozonation.

Responsible editor: Philippe Garrigues

✉ Beihai Zhou
zhoubeihai@sina.com

[1] Department of Environmental Engineering, School of Civil and Environmental Engineering, University of Science and Technology Beijing, Beijing 100083, China

Introduction

As a major fraction of natural organic matter (NOM) in surface water, humic acids (HAs) are notoriously known for their detrimental problems in treatment operations (Seredyńska-Sobecka et al. 2006). They turn not only the water into brown color (Wiszniowski et al. 2004) but also complex metals and organic pollutants (Terbouche et al. 2011; Wei et al. 2011). Moreover, they can react with active chlorine when water was treated in the plants for sterilization, resulting in the formation of trihalomethanes (Ghouas et al. 2012; Wei et al. 2011).

In the past decades, much effort has been devoted to the degradation of HAs. UV photocatalytic ozonation progress, which is characterized by the generation of very reactive hydroxyl radicals (·OH), has emerged as a highly efficient method for the decomposition of pollutants (Ghouas et al. 2012; Lin and Lin 2007). TiO_2 nanotubes (TNTs) have been considered as one of the most promising catalysts for eliminating environment contaminants in water (Carbajo et al. 2014) due to its advantages on long-term stability, large specific surface area, inexpensive, and non-toxic (Ghouas et al. 2012; Pang and Abdullah 2012a). However, it suffers from the wide energy band gaps (3.2 or 3.0 eV for the anatase or rutile phase, respectively) and fast recombination rate of charge carriers problems (Wang et al. 2008). To solve these problems, ions have been doped into TiO_2 (Shon et al. 2009). Among a great variety of ion dopants investigated previously, Fe^{3+} has been found to be the best candidate due to its proper band gap (~2.6 eV) and similar size to that of Ti^{4+} (Wang et al. 2011). In addition, Fe^{3+} ions trapped not only electrons (e^-) but also holes (h^+) (Shon et al. 2009), which leads to the increase of photocatalytic activity due to the production of ·OH (Pang and Abdullah 2012b; Yuan et al. 2014).

However, there are some drawbacks in using TNTs in powder form. First, the separation of TiO_2 from water is difficult

🙌 Springer

(Calza et al. 1997); second, the suspended TiO_2 tends to aggregate especially at high concentrations, and therefore, its photocatalytic activity decreased (Asiltürk and Şener 2012). This deficiency can be avoided by coating TiO_2 on inert substrates including glass, ceramsite, and stainless steel (Mansilla et al. 2007). But, the photocatalytic ability may decrease because the catalysts anchored on the substrate are difficult to effectively disperse in water to full contact with target pollutants (Shi et al. 2012). To solve this problem, adsorbent substrates with large surface area are employed because the adsorption properties of substrates can compensate for the loss of the photocatalytic ability caused by immobilization and even improve the photocatalytic ability (Shi et al. 2012).

Amongst the adsorbent substrates, zeolite (Huang et al. 2008), activated alumina (Al_2O_3) (Nguyen et al. 2004; Zhang et al. 2005), and activated carbon (AC) (Asiltürk and Şener 2012; Puma et al. 2008) have been used. Zeolite is a promising support for TiO_2 photocatalyst because of its regular pores and channel sizes and good adsorption ability. TiO_2 supported by zeolite integrates the photocatalytic activity of TiO_2 with the adsorption properties of zeolite together, which induce a synergistic effect, resulting in the enhancement of photocatalytic efficiency (Huang et al. 2008). Al_2O_3 is a good candidate due to its mechanical toughness and heat durability (Zhang et al. 2005). Using AC as a catalyst support will help increase the photodegradation rate by progressively allowing an increased quantity of substrate to come in contact with the TiO_2 through means of adsorption (Puma et al. 2008).

TiO_2 and adsorptive substrates have been efficiently associated by mechanical mixing of these two powders (Reddy et al. 2008; Takeuchi et al. 2009). However, study on preparation of the substrate-supported Fe^{3+}-doped TiO_2 nanotubes (Fe-TNTs) was limited. In this study, Fe-TNTs containing Fe^{3+} ions of 1.0 atomic percent (at.%) were successfully synthesized using hydrothermal method, and the substrates, including ceramsite, zeolite, Al_2O_3, and AC, were added. The catalytic properties of the photocatalysts were analyzed, and the photocatalytic activity and repeatability for the degradation of HAs by O_3/UV/substrate-supported Fe-TNT method were investigated. Control experiments were conducted to investigate the effects of O_3, O_3/UV, bare AC, O_3/UV/AC, O_2/UV/ceramsite-supported Fe-TNTs and O_2/UV/AC-supported Fe-TNT processes on HA removal, and the mechanism of HA degradation by O_3/UV in the presence of AC-supported Fe-TNTs was also discussed.

Materials and methods

Materials

P-25 TiO_2 was provided by the Degussa Corporation (Richfield Park, New Jersey). The powder has a Brunauer-Emmett-Teller (BET) surface area (S_{BET}) of 50 m^2/g, an average crystallite size of 21 nm, and a crystal structure of 80 % anatase and 20 % rutile. $Fe(NO_3)_3 \cdot 9H_2O$ (A.R.) was purchased from Beijing Chemical Reagent Company (China). HA solution was prepared by dissolving 1 g of HAs (A.R., molecular weight 2000–5000, pH 5–7, content>99 %, Tianjin Fuchen Chemical Reagent Company, China) in 10 mL NaOH solution and then diluted to 1000 mL.

Ceramsite, zeolite, Al_2O_3, and AC were all purchased from Tianjin Fuchen Chemical Reagent Company. Ceramsite was used as the inert substrate, while the others were adsorbent substrates. Al_2O_3 and AC were analytical reagents. The zeolite was made from pottery clay, silica sand, and $CaCO_3$, and its main components include SiO_2 (38.10 %), Al_2O_3 (33.76 %), Na_2O (10.19 %), CaO (6.53 %), and other materials such as water (11.42 %).

The major photocatalytic reactor is a cylindrical glass column with a diameter and height of 100 and 380 mm, respectively. An 18 W low-pressure mercury vapor lamp (Φ 22× 356 mm; UV radiation intensity 48–54 μW/cm^2; Beijing Haili Lighting Equipment Company, China) is found inside the reaction column. The UV wavelength range of the lamp was 250–260 nm, with the main wavelength of 254 nm. O_2 gas was prepared by an oxygenerator (Beijing North Star Yaao Scitech Co., Ltd, China), whereas O_3 was produced using O_2 by an O_3 generator (Beijing Tonglin Scitech Co., Ltd, China). O_3-containing gas was fed into the reactor through a porous glass core aeration plate (pore size 4–7 μm).

Preparation of the substrate-supported Fe-TNTs

One gram of P-25 TiO_2 and 0.0505 g of $Fe(NO_3)_3 \cdot 9H_2O$ were added into 16 mL of a 10 mol/L NaOH aqueous solution in a Teflon vessel. The mixture was stirred for 2 h at room temperature to form a suspension. Afterward, the suspension was heated at 110 °C for 24 h in an oven and cooled to room temperature in air. The precipitates were washed with distilled water to pH 7 and subsequently dispersed in a 0.1 mol/L HCl aqueous solution. After ultrasonication for 30 min, the precipitate was washed continuously with distilled water to pH 7. After filtration, Fe^{3+}-doped titanic acid nanotubes were obtained. The titanic acid nanotubes were dried in a hot air oven at 60 °C.

Ceramsite, zeolite, Al_2O_3, and AC were crushed into small particles (100–150 mesh) and soaked in a 5 % HCl solution for 12 h to remove any impurity. The acid solution was removed by filtration, and then, the substrates were washed with distilled water repeatedly to pH 7. Different substrate-supported Fe-TNT catalytic systems were prepared by mixing respective substrates with Fe^{3+}-doped titanic acid nanotubes using dry ethanol. The mass percent of Fe-TNTs in supporting substrates was ensured to be 1.0 % by weighting. The suspended substance were dried overnight in a hot air oven

at 60 °C after ultrasonication for 30 min. Fe-TNTs supported by different substrates were prepared by calcining the as-prepared catalysts at 500 °C for 2 h.

Characterization of the substrate-supported Fe-TNTs

The transmission electron microscopic (TEM) images were acquired with a HITACHI HT-7700 electron microscope (Tokyo, Japan). Scanning electron microscopic (SEM) images were obtained with an EVO18 electron microscope (Carl Zeiss, Germany), and atlases of energy distribution were achieved with a Tracor Northern 524 X-ray energy-dispersive spectrometer (EDS, USA). The surface elemental compositions of the Fe-TNTs were recorded with an X-ray photoelectron spectroscopy (XPS, AXIS ULTRA^{DLD}, Kratos Analytical, UK). X-ray diffraction (XRD) patterns of the substrate-supported catalysts were collected in a Rigaku Dmax-RB diffractometer (Tokyo, Japan). The S_{BET} were determined by N_2 adsorption on a Quadrasorb SI-MP apparatus (Quantachrome Instrument, USA). The diffuse reflectance spectroscopy (DRS) analyses were obtained using a HITACHI U-3010 UV-vis scanning spectrophotometer (Tokyo, Japan).

Photocatalytic activity tests

Aqueous slurries were prepared by adding 25 g of the photocatalyst to 2500 mL of a 10 mg/L HA aqueous solution at pH 7. Irradiation was performed using the 18 W UV lamp. The aqueous slurries were stirred by a magnetic stirring apparatus at 100 r/min, irradiated, and bubbled with O_3 (1 L/min, 10 %) for 30 min. The reaction was stopped at 5-min intervals by adding 0.5 mL of a 0.001 mol/L $Na_2S_2O_3$ solution into 50 mL of the sample (Yuan et al. 2013). Clear solution was obtained after centrifugation at 2000 r/min. The HA concentrations were analyzed using a UV-vis spectrophotometer (Hach DR5000, USA) at a wavelength of 254 nm (UV_{254}, / cm). According to the standard curve, the relation between the HA concentration ($C_{(HAs)}$, mg/L) and UV_{254} is $C_{(HAs)}=UV_{254}/0.0245$. After the test, precipitants in the reactor and the samples were washed with distilled water and dried at 60 °C. The tests were repeated for several times to investigate the repeatability of the catalysts. The HA removal efficiencies in the presence of unsupported Fe-TNTs were also investigated following the aforementioned methods, except that 0.25 g of the Fe-TNTs was invited instead of 25 g of the substrate-supported catalysts. The tests were repeated three times to minimize the errors.

Six comparative experiments were also conducted to investigate the effects of O_3, O_3/UV, bare AC, O_3/UV/AC, O_2/UV/ceramsite-supported Fe-TNTs, and O_2/UV/AC-supported Fe-TNT processes on HA removal. In the first experiment, only O_3 was inlet into the water without adding the catalyst, and the

UV lamp was turned off. In the second one, the O_3 generator and the UV lamp were both turned on. In the third experiment, 25 g of AC were added without turning on the O_3 generator and UV lamp. In the fourth experiment, the bare AC was added instead of AC-supported Fe-TNTs, and the O_3 generator and the UV lamp were both turned on. In the fifth and sixth experiments, all procedures were similar to the O_3/UV/substrate-supported Fe-TNT experiments except that the O_3 generator was turned off.

Results and discussion

Characterization of the photocatalysts

XPS analysis for the Fe-TNTs

The XPS spectra of the unsupported Fe-TNTs are shown in Fig. 1. Figure 1a shows the XPS survey scan of the 1.0 at.% Fe-TNTs. The sharp XPS peaks for Ti, O, Fe, Na, and C were observed. The C element in the result was mainly attributed to carbon contamination during the transfer of the samples to the XPS device (Stranak et al. 2010). The Na 1 s peak is due to the incomplete exchange of protons with Na^+ during acid washing with HCl (Pang and Abdullah 2012b).

Figure 1b, c shows the high-resolution XPS spectra of Fe 2p and Ti 2p, respectively. It can be seen from Fig. 1b that the binding energies of Fe 2p3/2 and Fe 2p1/2 for Fe-TNT samples were 710.4 and 723.9 eV, respectively, which were different from those for Fe_2O_3 (710.7 and 724.2 eV, respectively), illustrating that the Fe^{3+} ions were inbuilt in the lattice. In addition, the difference between the doublet peak (Fe2p3/2 and Fe2p1/2) is the same for the Fe^{3+} doped in lattice and present in Fe_2O_3, which indicates that the chemical valence of Fe element in Fe-TNTs was +3. Figure 1c indicates the Ti 2p3/2 and Ti 2p1/2 spin-orbital splitting photoelectrons for the undoped samples located at 458.7 and 464.4 eV, while those for Fe-TNTs were 458.5 and 464.2 eV, respectively. The binding energy difference between Ti 2p3/2 and Ti 2p1/2 remained to be 5.7 eV when Fe^{3+} ions were doped, which is the standard binding energy for Ti element (Mo and Ye 2009). The binding energies of Ti 2p becomes lower in Fe-TNTs when compared with pure TNTs because some Ti^{4+} ions are replaced by Fe^{3+} to increase the charge density of Ti. Although there were small differences in the binding energies of Ti 2p, these observations indicate that Ti was in the form of Ti^{4+} in the doped photocatalyst (Yalçin et al. 2006; Zhu et al. 2006). The shift of electrons' binding energy indicated the successful Fe^{3+} incorporation into the lattice of TNTs to form Ti-O-Fe bonds in the sample (Pang and Abdullah 2012b; Zhu et al. 2006). The electrons in the conduction band of TiO_2 may have transferred to Fe^{3+} in TiO_2, which resulted in a decrease in the outer electron cloud density of Ti^{4+} ions (Li et al. 2011).
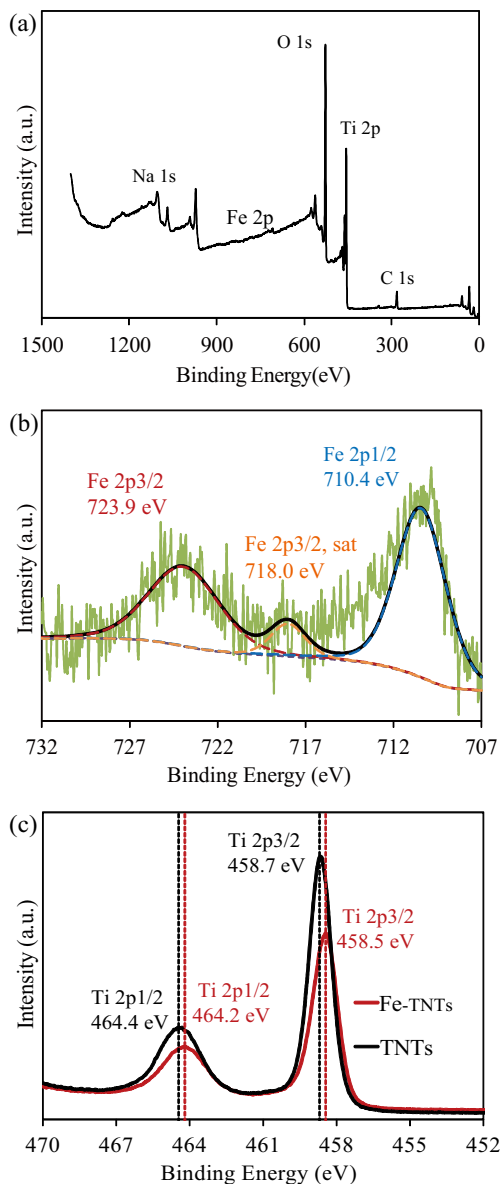
(a)

(b)

(c)

Fig. 1 XPS patterns of Fe-TNTs calcined at 500 °C: **a** survey scan; **b** and **c** spectra of Fe 2p and Ti 2p

UV-vis DRS analysis of the Fe-TNTs

The UV-vis DRS spectrograms of the 500 °C calcined unsupported pure TNTs and Fe-TNTs are shown in Fig. 2. The UV-vis DRS analysis of the catalyst was conducted to obtain the energy band gaps (E_g). TiO_2 had an indirect band gap, and plots relation is used:

$$F(R_\infty)h\gamma = A\left(h\gamma\text{-}E_g\right)^2 \quad (1)$$

where $F(R_\infty)$ is the Kubelka-Munk (K-M) function, h is the Planck constant, and γ is the frequency. The value of $F(R_\infty)$ is estimated using the K-M formula:

$$F(R_\infty) = \frac{(1\text{-}R_\infty)^2}{2R_\infty} \quad (2)$$

where R_∞ is the diffuse reflectance. The plots of E_g were deduced from the intersection of the linear portion extrapolation with the energy axis as depicted in Fig. 2 (inset).

The E_g of pure TNTs was 3.23 eV, which is slightly higher than that of anatase TiO_2 (3.2 eV) in the TiO_2 powder because of the quantum size effects on the different catalyst morphologies. The E_g of the Fe-TNTs (3.06 eV) was visibly narrower compared with that of pure TNTs. The result reveals that the doped elements involved were indeed incorporated into the lattice of TNTs, thus altered its crystal and electronic structures (Yu et al. 2009). The reduction in E_g of TNTs would allow the excitation of the catalyst under lower power of irradiation and therefore enhance the photocatalytic activity of the catalyst (Pang and Abdullah 2013). The values of the E_g are the same regardless of the supporting substrates, because the substrates have no influence on the optical properties of TNTs.

Morphologies of the catalysts

TEM and SEM were employed to observe the morphologies of the catalysts (Fig. 3). The morphologies of 1.0 at.% Fe-TNTs calcined at 500 °C is shown in Fig. 1a, indicating that the Fe-TNTs had an average diameter of about 6 nm with a hollow structure and open ends. Figure 1b–e shows the SEM images and EDS spectra of the substrate-supported catalysts. From the SEM images and the EDS spectra results, it was evident that the Ti and Fe elements were involved in the EDS spectra of the substrate-supported Fe-TNTs and that these elements were obtained from the Fe-TNTs which were coated on the surface of the supporting substrates.

XRD analysis for the catalysts

Figure 4 shows the XRD patterns of the catalysts. The crystallite phase containing iron oxide was not observed in the XRD pattern of the Fe-TNTs in Fig. 4a. For Fe-TNTs, the XRD peaks at 24.92° and 27.38° correspond to the characteristic peaks of the (101) crystal plane of anatase and the (110) crystal plane of rutile, respectively, while the (101) plane for
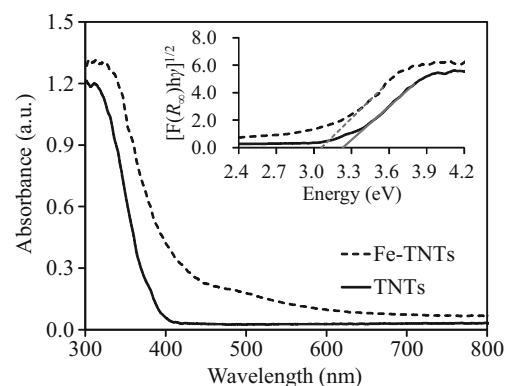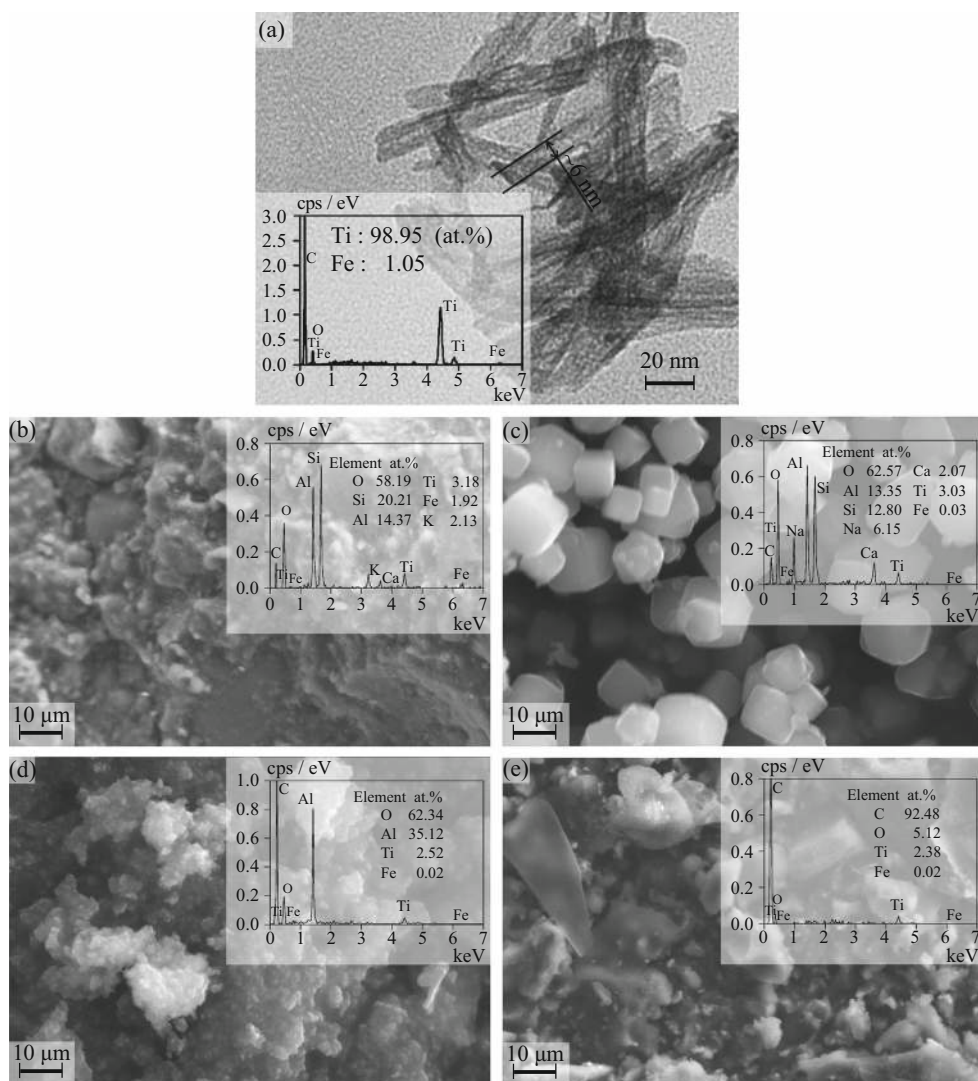

Fig. 2 DRS and E_g of 500 °C calcined unsupported TNTs and Fe-TNTs

Fig. 3 Morphologies and EDS of the catalysts. **a** TEM image and EDS of Fe-TNTs calcined at 500 °C, **b**–**e** SEM images and EDS of ceramsite-, zeolite-, Al_2O_3-, and AC-supported Fe-TNTs calcined at 500 °C, respectively

undoped TNTs was 25.30°. The Bragg angles (2θ) decreased when ions were added, which is consistent with the result of Teoh et al. (Teoh et al. 2007). This was because the ionic radius of Fe^{3+} was 0.64 Å, and it was possible for Fe^{3+} to diffuse through 0.77 Å channels along the c-axis to substitute Ti^{4+} in the TiO_2 lattice (Deng et al. 2009). The doped ions could have been highly dispersed in the TNTs (Choi et al. 2007; Pang and Abdullah 2012b). As a result, broadening diffraction peaks and decreasing peak intensities were observed.

It also can be seen from Fig. 4 that the peak intensities changed when TiO_2 was coated on the supporting substrates. The peak intensities of TiO_2 increased, and the intensities of the representative peaks of the supporting substrates decreased. It clearly illustrated that the substrate-supported Fe-TNT catalysts were successfully synthesized, and the Fe-TNTs were loaded on the surface of the supporting substrates.

The crystallinities of the catalysts before and after the HA photocatalytic degradation obey an almost similar pattern. It indicates that the catalysts are stable since the structure of those catalysts did not change after reaction (Reddy et al. 2003). However, the XRD peak intensities of the used substrate-supported Fe-TNT catalysts were somewhat lower than that of the fresh catalysts. This is because the pollutants were adsorbed on the catalysts, and the Fe-TNTs on the surface of the catalysts were abraded by a little when the solution was bubbled with O_3.

BET surface analysis for the catalysts

The S_{BET} of the substrate-supported Fe-TNTs are shown in Table 1. It can be seen that the composites of substrate-supported Fe-TNTs exhibited higher S_{BET} values than the unsupported Fe-TNTs. These features increased their photocatalytic performance (Li et al. 2012).

The ceramsite is not capable of adsorbing the pollutant in the solution because of its small S_{BET}. However, for zeolite, Al_2O_3, and AC, the Fe-TNTs on the

Fig. 4 XRD patterns of fresh and used catalysts. **a** XRD patterns of unsupported Fe-TNTs; **b**–**e** XRD patterns of ceramsite-, zeolite-, Al$_2$O$_3$-, and AC-supported Fe-TNTs calcined at 500 °C, respectively. "*A*" refers to the anatase phase, and "*R*" refers to the rutile phase
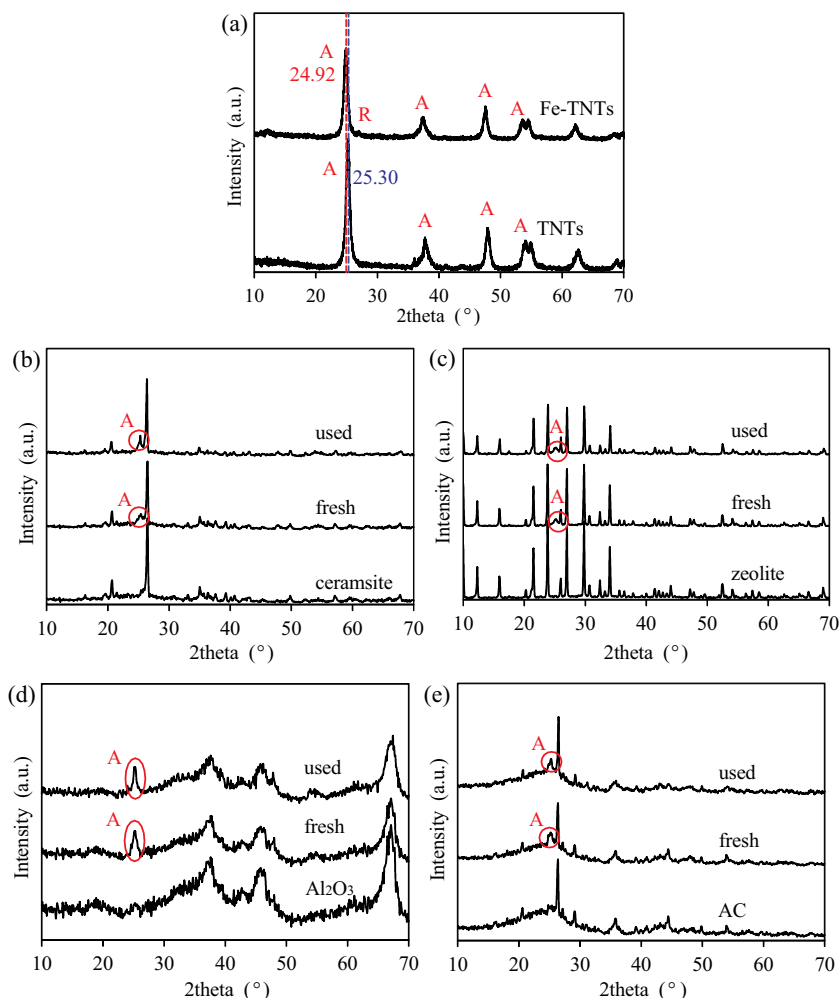
supporting substrates led to a decrease in the specific surface area. There were three possible reasons. First, the crystal size of Fe-TNTs was smaller than the pore size of the macropores and some of the mesopores, so the entrance of TiO$_2$ into the pores was possible. Second, Fe-TNTs could block the gates of the micropores and deposit on the surface of the catalysts (Asiltürk and Şener 2012). Thirdly, the decreasing in S_{BET} could be attributed to the agglomeration of small size crystallites when the catalysts were calcined at 500 °C (Lafjah et al. 2011).

Table 1 The S_{BET} (m^2/g) of the unsupported and substrate-supported Fe-TNTs

Type of substrates	Bare	Fresh	Used
Fe-TNTs	Non-existent	156.25	155.19
Ceramsite	3.21	2.55	3.13
Zeolite	570.03	371.57	365.61
Al$_2$O$_3$	262.26	170.42	165.85
AC	1150.37	489.69	480.18

It should be noted that the S_{BET} of AC-supported Fe-TNTs was larger than other catalysts because the pore structure of AC was well developed. The pores of the catalysts were not blocked by TiO$_2$ completely, and this created an opportunity for HAs and the intermediates of its degradation to be adsorbed.

The S_{BET} of ceramsite-supported Fe-TNTs after reaction was higher than that before reaction, possibly because of the small amount of Fe-TNTs separated from the ceramsite-supported catalyst. The S_{BET} of the zeolite-, Al$_2$O$_3$-, and AC-supported catalysts slightly decreased during the reaction, and it indicated that the amount of adsorption sites of the catalysts reduced because some of the pollutant was adsorbed into the catalysts.

Photocatalytic activity of the photocatalysts

The photocatalytic activities of the unsupported and substrate-supported Fe-TNTs were evaluated through the photocatalytic degradation of HAs under UV irradiation, as shown in Fig. 5.
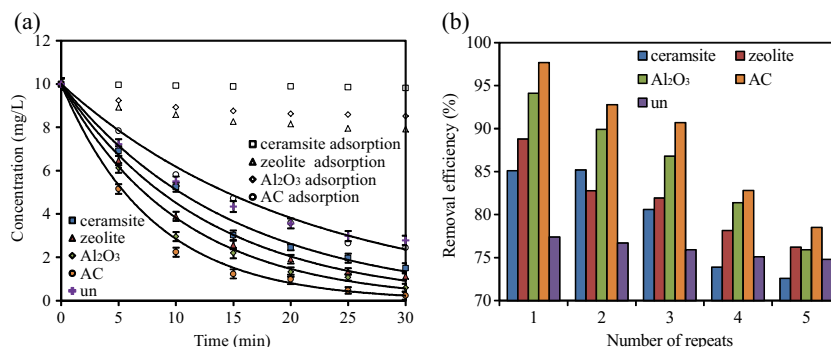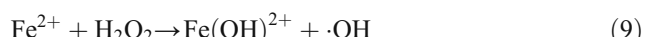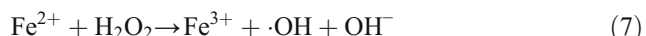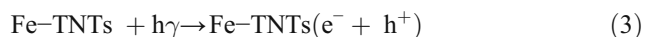
Fig. 5 Degradation of 10 mg/L HAs in the presence of unsupported and substrate-supported Fe-TNTs: **a** O_3/UV/substrate-supported catalyst degradation or substrate adsorption of HAs versus irradiation time for the fresh substrate-supported catalysts; **b** removal efficiencies of HAs for the repeatedly used catalysts. "*Ceramsite*," "*zeolite*," "*Al₂O₃*," and

"*AC*" stand for the supporting substrates, while "*un*" stands for the unsupported catalyst. *Error bars* represent the standard deviation of triplicate observations. Exactly 10 g/L of the substrate-supported catalysts or 0.1 g/L of the unsupported Fe-TNTs were used. The samples were irradiated and bubbled with O_3 (1 L/min, 10 %) for 30 min

The effect of Fe-TNTs

The HA removal efficiency in the presence of the unsupported Fe-TNT catalyst calcined at 500 °C was 77.2 %, and the number did not decrease significantly when the catalyst was used for several times (74.8 % for the Fe-TNTs used for the fifth time). High HA removal efficiency was achieved because during UV irradiation, the dissipated energy excited the Fe-TNT catalyst. A valence band e^- was promoted to the conduction band and left h^+ at the valence band [Eq. (3)] (Pang and Abdullah 2013). The h^+ reacted with H_2O to yield $\cdot OH$ [Eq. (4)]. Fe^{3+} in the ion-doped TiO_2 acted as shallow trapping sites for charge carriers [Eqs. (5)–(6)] and then reacted with H_2O_2 and OH^- in water to generate $\cdot OH$ [Eqs. (7)–(10)] (Wei et al. 2011) which is a powerful oxidizing agent that can attack HAs at or near the TiO_2 surface. Therefore, HAs were effectively removed from the water.

$$Fe-TNTs + h\gamma \rightarrow Fe-TNTs(e^- + h^+) \qquad (3)$$

$$h^+ + H_2O \rightarrow \cdot OH + H^+ \qquad (4)$$

$$Fe^{3+} + e^- \rightarrow Fe^{2+} \qquad (5)$$

$$Fe^{3+} + h^+ \rightarrow Fe^{4+} \qquad (6)$$

$$Fe^{2+} + H_2O_2 \rightarrow Fe^{3+} + \cdot OH + OH^- \qquad (7)$$

$$Fe^{4+} + OH^- \rightarrow Fe^{3+} + \cdot OH \qquad (8)$$

$$Fe^{2+} + H_2O_2 \rightarrow Fe(OH)^{2+} + \cdot OH \qquad (9)$$

$$Fe(OH)^{2+} + h\gamma \rightarrow Fe^{2+} + \cdot OH \qquad (10)$$

The effect of the supporting substrate type

The removal efficiency of HAs was 85.1 % when ceramsite-supported catalyst was used. The catalyst had a S_{BET} of only 2.55 m²/g, indicating that it was not capable of adsorbing HAs (1.8 % HA removal by ceramsite adsorption in the period of

30 min). Therefore, the HAs was degraded only by UV/Fe-TNT photocatalytic ozonation. Better photocatalytic activity was achieved when the Fe-TNTs were coating on the surface of the ceramsite substrate because the aggregation of the Fe-TNTs was partially avoided (Mansilla et al. 2007).

The HA removal efficiencies of zeolite, Al_2O_3, or AC adsorption in 30 min were 20.8, 14.8, and 75.6 %, respectively, indicating that the pollutants in the water could be adsorbed by the substrate-supported catalysts. The removal efficiencies by O_3/UV/substrate-supported catalysts, which were 88.8, 94.1, and 97.4 % for the zeolite-, Al_2O_3-, and AC-supported Fe-TNTs, were much higher than those by substrate adsorption.

Compared with the ceramsite-supported Fe-TNTs, the zeolite-, Al_2O_3-, and AC-supported catalysts had higher photocatalytic activities because of their larger S_{BET}. The residence time and concentration of the HA molecules close to the active Fe-TNT catalyst was artificially increased due to the presence of the highly adsorbent supporting substrates (Lafjah et al. 2011). This is in relation with the "adsorb and shuttle" concept, in which the adsorbent are used for adsorbing the pollutant before releasing to the neighboring photocatalytic sites (Lafjah et al. 2011). The onstream continuous regeneration of the adsorption sites of the zeolite, Al_2O_3, and AC occurred due to the intimate contact between both adsorption and photocatalytic sites. This regeneration was proposed to occur through the "remote degradation" mechanism, based on the surface diffusion of active oxidizing chemical species from the Fe-TNTs, where they were formed, to the adsorbent sites on which the pollutants were adsorbed (Lafjah et al. 2011). In addition, in contrast to the Fe-TNTs and the supporting substrates mixing, the intimate contact between the supporting substrates and Fe-TNTs could allow the transfer of the excited electrons from the Fe-TNT conduction band to the surface of the supporting substrates to be effective, and thus, the e^--h^+ recombination rate decreased (Mahalakshmi et al. 2009).

The degradation of HAs was consistent with a pseudo-first-order kinetic. Highest photocatalytic activity was obtained in

the presence of AC-supported Fe-TNTs, as HAs was removed by 97.4 %, with rate constant of 0.126/min. The reason was that the AC-supported Fe-TNTs had the largest S_{BET}, so more HAs could be adsorbed by the catalysts.

The pH values of water before and after the reaction were measured. The results show that the pH decreased from 6.55–6.95 to 4.69–4.85, indicating the formation of carboxylic acids which are oxidation-resistant compounds during the photocatalytic ozonation process.

The effect of the number of repeats

Experimental studies were performed to investigate the repeatability of the catalysts by using the used catalysts for several times. The results show that the removal efficiencies of HAs reduced slightly as the number of repeats increased, with the HA removal efficiencies in the presence of the ceramsite supported, the zeolite supported, the Al_2O_3 supported, or the AC-supported Fe-TNTs which was used for five times were 72.6, 76.2, 75.9, or 78.5 %, respectively. The reason was that the pollutant was adsorbed into the adsorbent, and some of the pollutant did not release to the photocatalytic sites. The amount of adsorption sites decreased when the catalysts was used repeatedly. It could also be seen from Table 1 that the S_{BET} of fresh zeolite-, Al_2O_3-, and AC-supported catalysts was smaller than those of used catalysts because of the adsorption of HAs.

After the catalyst was used for five times, the removal efficiency of HAs in the presence of AC supported catalyst was still sufficient in water treatment.

Mechanism of HA degradation by AC-supported Fe-TNTs

The O_3, O_3/UV, AC, O_3/UV/AC, O_2/UV/ceramsite-supported Fe-TNTs and O_2/UV/AC-supported Fe-TNT processes

Control experiments were conducted to investigate the effects of O_3, O_3/UV, bare AC, O_3/UV/AC, O_2/UV/ceramsite-supported Fe-TNTs, and O_2/UV/AC-supported Fe-TNT processes on HA removal, and the results were compared with those of O_3/UV/ceramsite-supported Fe-TNTs and O_3/UV/AC-supported Fe-TNT processes (Fig. 6).

Figure 6 shows that 28.8 to 29.6 % of HAs was removed after ozonation, whereas the removal efficiencies were 31.5–32.2, 52.4–87.1, or 40.1–54.0 % for O_3/UV, O_3/UV/AC, or O_2/UV/ceramsite-supported Fe-TNT processes. For O_3/UV process, the ·OH production by ozonation was enhanced in the presence of UV light with λ below 310 nm [Eqs. (11) and (12)] (Wei et al. 2011). For O_2/UV/ceramsite-supported Fe-TNT process, during UV irradiation, the Fe-TNT catalyst can promote the decomposition of HAs [Eqs. (3)–(10)]. The lower HA decomposition rate of ozonation compared with those of
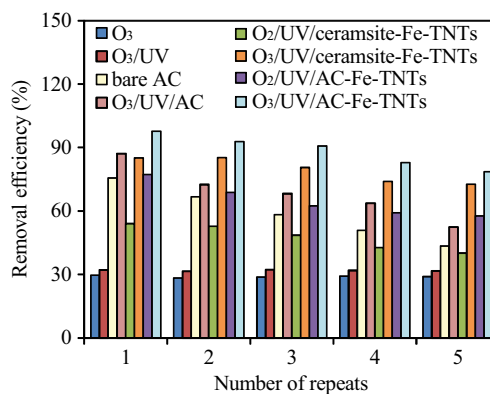

Fig. 6 Degradation of 10 mg/L HAs by O_3, O_3/UV, bare AC, O_3/UV/AC, O_2/UV/ceramsite-supported Fe-TNTs, O_3/UV/ceramsite-supported Fe-TNTs, O_2/UV/AC-supported Fe-TNTs, and O_3/UV/AC-supported Fe-TNT processes. Exactly 10 g/L of the substrate-supported catalysts were used. The samples were irradiated and bubbled with O_3 (1 L/min, 10 %) for 30 min

the other two processes is due to the lower oxidizability of O_3 compared with that of the ·OH (Mansilla et al. 2007).

$$O_3 + H_2O + h\gamma \rightarrow O_2 + H_2O_2 \qquad (11)$$

$$2O_3 + H_2O_2 \rightarrow 2 \cdot OH + 3O_2 \qquad (12)$$
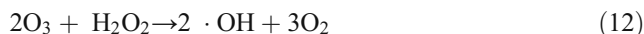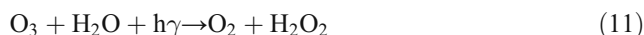
The removal efficiency by O_2/UV/ceramsite (AC)-supported Fe-TNT process was significantly lower than that of O_3/UV/ceramsite (AC)-supported Fe-TNT process. These results indicate that HA removal over UV photocatalytic oxygenation can be enhanced by ozonation.

The photocatalytic activity of AC-supported Fe-TNTs was much higher than that of ceramsite-supported catalyst. Since the photocatalytic experiments were performed under the same conditions, the enhanced activity could be related to the adsorption of AC (Liu et al. 2007). The removal efficiency of HAs by O_3/UV/AC-supported Fe-TNT process was higher than those of bare AC adsorption or O_3/UV/AC process, especially when the AC was used for five times. That indicated the continuous adsorption of HAs and regeneration of the adsorption sites of AC in the presence of Fe-TNTs coated on the surface of AC. However, strong adsorption of pollutant molecules may inhibit subsequent photocatalytic reactions. As the number of repeats of the catalysts increased, the HA removal efficiencies reduced.

Mechanism of HA degradation

The enhanced photocatalytic activity of AC-supported Fe-TNTs was related to a synergistic effect of ozonation, AC adsorption, and Fe-TNT photocatalysis. A proposed mechanism for the HA removal is shown in Fig. 7.

AC had a well-developed pore structure with very large S_{BET} and adsorption capacity. It possessed large numbers of active adsorption sites; thus Has, were adsorbed before
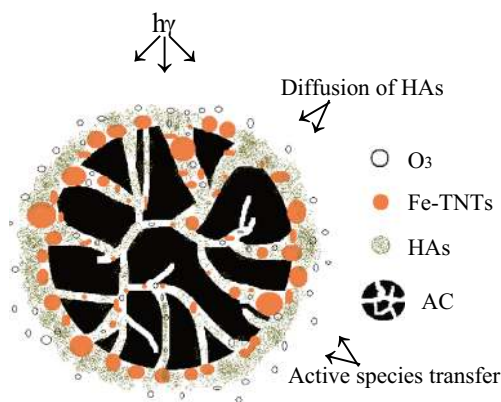
Fig. 7 Mechanism of HA degradation by O_3/UV/AC-supported Fe-TNT process

transferring to the decomposition center of Fe-TNTs (Wang et al. 2009). An important step in the photocatalytic process is the adsorption of HAs on the surface of AC. For a pseudo-first-order reaction, the higher the concentration of the pollutant is, the faster the reaction rate is. The concentration of HAs adsorbed by AC was much higher than that in the water; therefore, the reaction was accelerated. As the HAs were degraded in the presence of AC-supported Fe-TNTs, the HA amount on the Fe-TNT surface decreased, so that the HA molecules adsorbed were desorbed from AC. Because of the O_3/UV/Fe-TNT process, the adsorption sites were released and the adsorption capacity of AC was regenerated. Thus, the HA degradation was achieved through a synergistic mechanism of AC adsorption and Fe-TNT photocatalytic ozonation (Wang et al. 2009).

Conclusions

In this study, Fe-TNTs were successfully synthesized using hydrothermal method. AC was found to be better supporting substrate for Fe-TNTs than ceramsite, zeolite, and Al_2O_3 on the photocatalytic degradation of HAs under O_3/UV condition. A removal efficiency of 97.4 % can be achieved in the presence of fresh AC-supported 1.0 at.% Fe-TNTs calcined at 500 °C. Furthermore, even after the AC-supported catalyst was used for five times, its removal efficiency of HAs was still sufficient in water treatment. The better photocatalytic activity of AC-supported Fe-TNTs could be related to its larger S_{BET}. However, the removal efficiencies of HAs reduced when the catalysts was used for more than once, since the amount of adsorption sites of the supporting substrates decreased. The enhanced photocatalytic activity of AC-supported Fe-TNTs was related to a synergistic effect of AC adsorption and Fe-TNT photocatalytic ozonation.

References

Asiltürk M, Şener Ş (2012) TiO2-activated carbon photocatalysts: preparation, characterization and photocatalytic activities. Chem Eng J 180:354–363

Calza P, Minero C, Pelizzetti E (1997) Photocatalytically assisted hydrolysis of chlorinated methanes under anaerobic conditions. Environ Sci Technol 31:2198–2203

Carbajo J, García-Muñoz P, Tolosana-Moranchel A, Faraldos M, Bahamonde A (2014) Effect of water composition on the photocatalytic removal of pesticides with different TiO2 catalysts. Environ Sci Pollut Res 21:12233–12240

Choi YJ, Seeley Z, Bandyopadhyay A, Bose S, Akbar SA (2007) Aluminum-doped TiO2 nano-powders for gas sensors. Sensors Actuators B Chem 124:111–117

Deng L, Wang S, Liu D, Zhu B, Huang W, Wu S, Zhang S (2009) Synthesis, characterization of Fe-doped TiO2 nanotubes with high photocatalytic activity. Catal Lett 129:513–518

Ghouas H, Haddou B, Kameche M, Derriche Z, Gourdon C (2012) Extraction of humic acid by coacervate: investigation of direct and back processes. J Hazard Mater 205–206:171–178

Huang M, Xu C, Wu Z, Huang Y, Lin J, Wu J (2008) Photocatalytic discolorization of methyl orange solution by Pt modified TiO2 loaded on natural zeolite. Dyes Pigments 77:327–334

Lafjah M, Djafri F, Bengueddach A, Keller N, Keller V (2011) Beta zeolite supported sol-gel TiO2 materials for gas phase photocatalytic applications. J Hazard Mater 186:1218–1225

Li X, Zou X, Qu Z, Zhao Q, Wang L (2011) Photocatalytic degradation of gaseous toluene over Ag-doping TiO2 nanotube powder prepared by anodization coupled with impregnation method. Chemosphere 83:674–679

Li F, Zhao Y, Hao Y, Wang X, Liu R, Zhao D, Chen D (2012) N-doped P25 TiO2-amorphous Al2O3 composites: one-step solution combustion preparation and enhanced visible-light photocatalytic activity. J Hazard Mater 239–240:118–127

Lin C, Lin KS (2007) Photocatalytic oxidation of toxic organohalides with TiO2/UV: the effects of humic substances and organic mixtures. Chemosphere 66:1872–1877

Liu SX, Chen XY, Chen X (2007) A TiO2/AC composite photocatalyst with high activity and easy separation prepared by a hydrothermal method. J Hazard Mater 143:257–263

Mahalakshmi M, Priya SV, Arabindoo B, Palanichamy M, Murugesan V (2009) Photocatalytic degradation of aqueous propoxur solution using TiO2 and Hβ zeolite-supported TiO2. J Hazard Mater 161:336–343

Mansilla HD, Mora A, Pincheira C, Mondaca MA, Marcato PD, Durán N, Freer J (2007) New photocatalytic reactor with TiO2 coating on sintered glass cylinders. Appl Catal B Environ 76:57–63

Mo D, Ye D (2009) Surface study of composite photocatalyst based on plasma modified activated carbon fibers with TiO2. Surf Coat Technol 203:1154–1160

Nguyen HT, Miao L, Tanemura S, Tanemura M, Toh S, Kaneko K, Kawasaki M (2004) Structural and morphological characterization of anatase TiO2 coating on χ-Alumina scale fiber fabricated by sol-gel dip-coating method. J Cryst Growth 271:245–251

Pang YL, Abdullah AZ (2012a) Comparative study on the process behavior and reaction kinetics in sonocatalytic degradation of organic

dyes by powder and nanotubes TiO$_2$. Ultrason Sonochem 19:642–651

Pang YL, Abdullah AZ (2012b) Effect of low Fe^{3+} doping on characteristics, sonocatalytic activity and reusability of TiO$_2$ nanotubes catalysts for removal of Rhodamine B from water. J Hazard Mater 235–236:326–335

Pang YL, Abdullah AZ (2013) Fe^{3+} doped TiO$_2$ nanotubes for combined adsorption–sonocatalytic degradation of real textile wastewater. Appl Catal B Environ 129:473–481

Puma GL, Bono A, Krishnaiah D, Collin JG (2008) Preparation of titanium dioxide photocatalyst loaded onto activated carbon support using chemical vapor deposition: a review paper. J Hazard Mater 157:209–219

Reddy EP, Davydov L, Smirniotis P (2003) TiO$_2$-loaded zeolites and mesoporous materials in the sonophotocatalytic decomposition of aqueous organic pollutants: the role of the support. Appl Catal B Environ 42:1–11

Reddy MP, Phil HH, Subrahmanyam M (2008) Photocatalytic disinfection of escherichia coli over titanium (IV) oxide supported on Hβ zeolite. Catal Lett 123:56–64

Seredyńska-Sobecka B, Tomaszewska M, Morawski AW (2006) Removal of humic acids by the ozonation-biofiltration process. Desalination 198:265–273

Shi JW, Cui HJ, Chen JW, Fu ML, Xu B, Luo HY, Ye ZL (2012) TiO$_2$/activated carbon fibers photocatalyst: effects of coating procedures on the microstructure, adhesion property, and photocatalytic ability. J Colloid Interface Sci 388:201–208

Shon HK, Cho DL, Na SH, Kim JB, Park HJ, Kim JH (2009) Development of a novel method to prepare Fe- and Al-doped TiO$_2$ from wastewater. J Ind Eng Chem 15:476–482

Stranak V, Quaas M, Bogdanowicz R, Steffen H, Wulff H, Hubicka Z, Tichy M, Hippler R (2010) Effect of nitrogen doping on TiO$_x$N$_y$ thin film formation at reactive high-power pulsed magnetron sputtering. J Phys D Appl Phys 43:1–9

Takeuchi M, Deguchi J, Hidaka M, Sakai S, Woo K, Choi PP, Park JK, Anpo M (2009) Enhancement of the photocatalytic reactivity of TiO$_2$ nano-particles by a simple mechanical blending with hydrophobic mordenite (MOR) zeolite. Appl Catal B Environ 89:406–410

Teoh WY, Amal R, Mädler L, Pratsinis SE (2007) Flame sprayed visible light-active Fe-TiO$_2$ for photomineralisation of oxalic acid. Catal Today 120:203–213

Terbouche A, Ramdane-Terbouche CA, Hauchard D, Djebbar S (2011) Evaluation of adsorption capacities of humic acids extracted from Algerian soil on polyaniline for application to remove pollutants such as Cd(II), Zn(II) and Ni(II) and characterization with cavity microelectrode. J Environ Sci 23:1095–1103

Wang J, Sun W, Zhang Z, Jiang Z, Wang X, Xu R, Li R, Zhang X (2008) Preparation of Fe-doped mixed crystal TiO$_2$ catalyst and investigation of its sonocatalytic activity during degradation of azo fuchsine under ultrasonic irradiation. J Colloid Interface Sci 320:202–209

Wang X, Liu Y, Hu Z, Chen Y, Liu W, Zhao G (2009) Degradation of methyl orange by composite photocatalysts nano-TiO$_2$ immobilized on activated carbons of different porosities. J Hazard Mater 169:1061–1067

Wang C, Shi H, Li Y (2011) Synthesis and characteristics of natural zeolite supported Fe^{3+}-TiO$_2$ photocatalysts. Appl Surf Sci 257:6873–6877

Wei MC, Wang KS, Hsiao TE, Lin IC, Wu HJ, Wu YL, Liu PH, Chang SH (2011) Effects of UV irradiation on humic acid removal by ozonation, Fenton and Fe$_0$/air treatment: THMFP and biotoxicity evaluation. J Hazard Mater 195:324–331

Wiszniowski J, Robert D, Surmacz-Gorska J, Mikscha K, Malatoc S, Weber J (2004) Solar photocatalytic degradation of humic acids as a model of organic compounds of landfill leachate in pilot-plant experiments: influence of inorganic salts. Appl Catal B Environ 53:127–137

Yalçın Y, Kılıç M, Çınar Z (2006) Fe^{+3}-doped TiO$_2$: a combined experimental and computational approach to the evaluation of visible light activity. Appl Catal B Environ 99:469–477

Yu J, Xiang Q, Zhou M (2009) Preparation, characterization and visible-light-driven photocatalytic activity of Fe-doped titania nanorods and first-principles study for electronic structures. Appl Catal B Environ 90:595–602

Yuan R, Zhou B, Hua D, Shi C (2013) Enhanced photocatalytic degradation of humic acids using Al and Fe co-doped TiO$_2$ nanotubes under UV-ozonation for drinking water purification. J Hazard Mater 262:527–538

Yuan R, Zhou B, Hua D, Shi C, Ma L (2014) Effect of metal-ion doping on the characteristics and photocatalytic activity of TiO$_2$ nanotubes for the removal of toluene from water. Water Sci Technol 69:1697–1704

Zhang X, Zhou M, Lei L (2005) Preparation of anatase TiO$_2$ supported on alumina by different metal organic chemical vapor deposition methods. Appl Catal A Gen 282:285–293

Zhu J, Chen F, Zhang J, Chen H, Anpo M (2006) Fe^{3+}-TiO$_2$ photocatalysts prepared by combining sol-gel method with hydrothermal treatment and their characterization. J Photochem Photobiol A Chem 180:196–204